Anisotropic features of natural Teguline clay

Feng Zhang, Yu Jun Cui, Ling-Ling Zeng, Nathalie Conil

Anisotropic features of natural Teguline clay

Feng Zhang[1], Yu-Jun Cui[1], Lingling Zeng[2], Nathalie Conil[3]

1: Ecole des Ponts ParisTech, Laboratoire Navier/CERMES, 6 et 8 avenue Blaise Pascal, 77455 Marne La Vallée cedex 2, France
2: Institute of Geotechnical Engineering, College of Civil Engineering, Fuzhou University, 350108 Fuzhou, China
3: CMHM, Andra, RD 960, 55290 Bure, France

***Corresponding author:**
Prof. Yu-Jun CUI
Ecole des Ponts ParisTech
6-8 av. Blaise Pascal, Cité Descartes, Champs-sur-Marne
77455 Marne-la-Vallée cedex 2
France

E-mail : yu-jun.cui@enpc.fr
Tel: + 33 1 64153550

Abstract: In general, due to their geological formation by deposition, natural stiff clays exhibit anisotropic thermo-hydro-mechanical behaviour. This behaviour is important to be considered in geological and geo-environmental engineering. In this study, natural stiff Teguline clay was extracted at different depths and the thermal conductivity, compressibility and hydraulic conductivity were determined on samples along various orientations with respect to the bedding plane. Significant thermal and hydraulic conductivity anisotropies were evidenced with higher values along the bedding plane, indicating that both heat and water transfers preferentially occurred along the direction parallel to the bedding plane. Moreover, the compression index in the horizontal direction were found lower than in the vertical direction, while opposite phenomenon was observed for the yield stress. The degrees of thermal conductivity anisotropy η_{T}, compression index anisotropy η_{Cc1}, yield stress anisotropy $\eta_{\sigma'_{\mathrm{y}}}$ and hydraulic conductivity anisotropy η_{k1} were found comparable, indicating that bedding is a good indicator of the inherent thermo-hydro-mechanical anisotropy for natural stiff clays. Upon loading in oedometer after the yield stress, the inherent anisotropy changed: for the vertical sample (loading direction normal to the bedding plane), loading led to more and more anisotropy, while for the horizontal sample (loading direction parallel to the bedding plane), the inherent anisotropy disappeared first; then, the induced anisotropy was developed. These findings provided useful information for analyzing the thermo-hydro-mechanical anisotropy of natural soils in geotechnical and geo-environmental engineering.

***Key words*:** Clays; Anisotropy; Thermal conductivity; Compressibility; Hydraulic

conductivity

Introduction

Due to their layered microstructure resulting from their initial deposition, natural stiff clays generally exhibit inherent anisotropy, which leads to directional dependence of their thermal, mechanical and hydraulic properties. This anisotropic feature is important to be accounted for while analysing the stability of the galleries excavated for geological nuclear waste disposal (Armand et al., 2013; François et al., 2014; Salehnia et al., 2015; Seyedi et al., 2017), because: i) during excavation, the damage of the host rock (thus the excavation damaged zone) is strongly depending on its anisotropy (Naumann et al., 2007; Niandou et al., 1997; Zhang et al., 2015); ii) after excavation, the stresses exerted to the concrete linings also strongly depend on the anisotropy by the surrounding host rock (Armand et al., 2013). This explains the particular attention paid recently to the anisotropic features of Boom Clay (Dao et al., 2014a; Dao et al., 2014b; Dao et al., 2015a; Dao et al., 2015b), Callovo-Oxfordian claystone (Armand et al., 2013; Zhang et al., 2015; Seyedi et al., 2017) and Tournemire shale (Niandou et al., 1997; Masri et al., 2014), and of Opalinus Clay (Naumann et al., 2007; Bertrand and Collin, 2017; Favero et al., 2018).

It has been well documented that for natural clays, the thermal conductivity and hydraulic conductivity in the horizontal direction are in general larger than in the vertical direction (Midttømme and Roaldset, 1999; Dao et al., 2014a), suggesting that the generally horizontal bedding planes are preferential flow directions for heat and fluids. Alshawmar (2014) carried out one-dimensional consolidation tests on undisturbed sensitive Champlain Sea clay and found that the ratio of horizontal to

vertical preconsolidation pressure varied from 0.71 to 0.95. Moreover, the horizontal compression index was 1% to 23%, higher than the vertical one, showing a larger compressibility in the horizontal orientation. This can be attributed to the directional differences in soil fabric and in stress history during soil sedimentation (Khan, 1993). The natural clays (such as Opalinus Clay) also exhibited anisotropic features in terms of strength with higher value in the direction parallel and perpendicular to the bedding plane and lower value in the direction at 45° to the bedding plane (Naumann et al., 2007).

It is also recognised that the anisotropic hydro-mechanical behavior is directly correlated to the microstructure features (Hicher et al., 2000; Zeng et al., 2017). Zeng et al. (2017) investigated the anisotropic swelling of Teguline clay associated with change in microstructure during wetting. The clay samples were allowed to swell freely or only in the vertical direction. The results showed that swelling occurred mainly in the direction perpendicular to the bedding plane, accompanied with the development of micro-fissures parallel to the bedding plane, the swelling along the bedding direction being negligible. The wetting-induced micro-fissures corresponded to the damage of soil, which could significantly modify the hydro-mechanical properties of soil in an anisotropic fashion.

Albeit the importance of anisotropy features recognised for natural soils from both academic and practical points of view, such results remain relatively limited, mainly because of the relatively large variability of natural soils that renders the interpretation of the test results difficult. This study aims at investigating the

anisotropy feature of the thermo-hydro-mechanical behaviour of natural clays. Natural Teguline clay was considered for this purpose and its thermal conductivity, compressibility and hydraulic conductivity was determined in various orientations with respect to the bedding plane, which allowed the inherent anisotropy to be identified. Furthermore, the development of stress-induced anisotropy beyond the yield stress was also analyzed.

Materials and methods

Test materials

Stiff Teguline clay samples were extracted from borehole AUB1011 at depths of 18.21 m and 31.76 m, also from borehole AUB1012 at depths of 5.46 m, 11.56 m, 18.06 m, 30.5 m, 30.8 m and 31.22 m, in the area of Albian Paris Basin (Aube, France), following the direction perpendicular to the bedding plane that was found to be parallel to the ground surface through observation of a piece of Teguline clay immersed in water. They were then covered by membrane and conserved in a fully confined cell (T1), preventing water loss and soil rebounding. This clay has a liquid limit of 42.0-56.5%, a plastic limit of 17.5-29.4% and a specific gravity of 2.71. The mineralogy was mainly defined by illite, illite-smectite, kaolinite, chlorite, quartz and carbonates (Zhang et al., 2018). The clay content and quartz content vary over depth, and their profiles are presented in Fig. 1. It can be observed that Teguline clay consists of 15-60% of clay minerals and 20-70% of quartz. It is worth noting that the tested Teguline clay cores were taken at the depths between 5 m and 40 m. The clay content

varied from 35% to 58% and the quartz content from 28% to 46%, showing a certain variability of mineralogy.

Thermal conductivity tests

After opening the Teguline clay from the fully confined cell (T1) in the laboratory, the samples were prepared by trimming to reach the dimensions of 85 mm in diameter and 60 mm - 90 mm in height. Then, they were covered by plastic film to avoid water loss by evaporation. The test program is presented in Table 1.

A thermal properties analyzer, KD2, was used to measure the thermal conductivity. Its principle is based on the transient hot-wire method. This device meets the requirements of ASTM Standards (ASTM D5334-00, 2000). In order to install the thermal probe into the soil, a hole was drilled in the centre of each sample. A layer of thermal grease was first applied on the surface of the probe to ensure a good contact between the soil and the probe. Then, the probe with grease was inserted into the sample. The thermal conductivity was measured in three orientations ($\theta = 0^{\circ}$, $\theta = 90^{\circ}$, and $\theta = 45^{\circ}$ to the bedding plane). For a better accuracy, five successive measurements were conducted and a mean value was considered for further analyses.

Due to the geological formation by deposition, the Teguline clay is considered as transversely isotropic material. In that case, the measured thermal conductivity λ_0 corresponds to that in the direction parallel to the bedding plane $\lambda_{//}$. However, in the case of $\theta = 90^{\circ}$, the measured thermal conductivity λ_{90} is not the value in the direction perpendicular to the bedding plane ($\lambda_{\perp}$). The true value of $\lambda_{\perp}$ was thus back calculated using the following equation:

146 $$\lambda_{\perp} = \frac{(\lambda_{90})^2}{\lambda_0} \quad (1)$$

147 Eq. (1) has been used by many authors (Penner, 1963; Munroe and Sass, 1987;
148 Davis et al., 2007; Dao et al., 2014a; Popov et al., 2012; Riche and Schneebeli, 2013;
149 Ye et al., 2017) to determine the thermal conductivity in the direction perpendicular to
150 the bedding plane $\lambda_{\perp}$ in different materials (snow, igneous rocks, clay sediments,
151 etc.).

152 The thermal conductivity of θ=45° was calculated by Eq. (2) (Dao et al., 2014a):

153 $$\lambda_{45} = \sqrt{\frac{(\lambda_0)^2 + (\lambda_{90})^2}{2}} \quad (2)$$

154 The thermal conductivity of clays depends on the composition (solid, water and
155 gas phases), the nature of the dominant minerals, the density and temperature (Farouki,
156 1986; Midttømme and Roaldset, 1999; Tang et al., 2008; Ye et al., 2017). The effect
157 of the slightly decrease of degree of saturation (S_r) of the studied samples was
158 accounted for according to the Johansen's method (Johansen, 1975; Farouki, 1986):

159 $$\lambda_{sat} = \frac{(\lambda - \lambda_{dry})}{K_e} + \lambda_{dry} \quad (3)$$

160 where λ_{sat}, λ and λ_{dry} expressed in W/(m·K) are respectively the thermal
161 conductivities at saturated state, unsaturated state and dry state; K_e is the Kersten's
162 number.

163 The Kersten's number (K_e) and the thermal conductivity at dry density λ_{dry} can
164 be determined by the following equations:

165 $$K_e \cong \log(S_r/100) + 1.0 \quad (4)$$

166 $$\lambda_{dry} = \frac{0.135\rho_d + 64.7}{\rho_s - 0.947\rho_d} \quad (5)$$

167 where S_r is the degree of saturation, ρ_d is the dry unit mass of soil and ρ_s is the unit
168 mass of solids, both expressed in kg/m^3.

169 The degree of thermal conductivity anisotropy η_T is defined as:

170 $$\eta_T = \frac{\lambda_{//}}{\lambda_{\perp}} \quad (6)$$

171 where $\lambda_{//}$ (equal to λ_0) and $\lambda_{\perp}$ were respectively the thermal conductivities in the
172 directions parallel and perpendicular to the bedding plane.

173 *Compressibility and hydraulic conductivity measurements*

174 The samples extracted from borehole AUB1012 at depths of 11.56 m and 30.5 m,
175 30.8 m were used for the compressibility and the hydraulic conductivity
176 measurements. Samples of 50 mm in diameter and 20 mm in height were prepared by
177 trimming from two directions: horizontal direction and vertical direction. The test
178 program is presented in Table 2.

179 After installing the soil sample in oedometer cell, step loading was applied up to
180 the in-situ effective vertical stress without putting the sample in contact with water in
181 order to avoid soil swelling which would affect the soil microstructure and thereby the
182 soil hydro-mechanical behavior (Delage et al., 2007; Cui et al., 2013). The in-situ
183 effective vertical stress σ'_{vo} was estimated using Eq. (7):

184 $$\sigma'_{v0} = \gamma h - u_0$$

185 (7)

186 where γ is the mean unit weight of the soil above the depth considered, h is the depth

of the soil core (see Table 2); u_0 is the in-situ pore pressure estimated from the ground water level that is assumed to be at the ground surface for simplicity (Zhang et al., 2018).

The value of σ'_{vo} for AUB1012 extracted at 11.56 m was found to be 0.125 MPa. This value was applied to the sample trimmed in the horizontal and the vertical directions (11.56 m). The values of σ'_{vo} for AUB1012 extracted at 30.8 m and 30.5 m were estimated at 0.34 MPa, which was applied to the sample trimmed in the horizontal (30.8 m) and the vertical (30.5 m) directions. It is worth noting that, experimentally, it is difficult to adopt an appropriate stress to be applied to the horizontal sample. Thus, for simplicity, the in-situ effective vertical stress applied to samples in both the horizontal and vertical directions. This also made the comparison between the responses of the samples in two directions easier.

After application of σ'_{vo}, the bottom porous stone and the drainage system were saturated with de-ionized water, and the sample was kept saturated for 1 week. Then, a constant water pressure of 0.1 MPa was applied using a controller of pressure/volume (CPV) from the lower base of the cell, and the upper base was kept at atmospheric pressure. Based on the water flux monitored, the hydraulic conductivity was determined by the constant-head method. Afterwards, the injection pressure of 0.1 MPa was reduced to 0.01 MPa, and the compression test was performed in a conventional way by step loading (see Table 2), up to 7.87 MPa for AUB1012 at depth of 11.56 m in two directions and 16.08 MPa for AUB1012 at depths of 30.80 m in the horizontal direction and 30.50 m in the vertical direction.

The hydraulic conductivity test was also performed after stabilization at each loading step. The axial displacement was monitored using a LVDT (Linear Variable Differential Transformer), and the deformation was considered as stabilized when the vertical strain rate was lower than 5×10^{-4} every 8 h (AFNOR, 1997). Note that the compression curve of vertical sample (where loading occurred in the direction normal to the bedding plane) from AUB1012 (11.56 m) was collected from Zhang et al. (2018).

All the tests were performed at a controlled temperature of 20 ± 1°C.

Experimental results

Thermal conductivity

Since the values of degree of saturation were slightly lower than 100%, the thermal conductivity values at saturated state were first calculated using Eqs. (3), (4) and (5). Figs. 2(a)-2(d) show the changes of thermal conductivity with dry density and water content along the three directions (λ_0, λ_{45}, λ_{90}) for samples AUB1011 and AUB1012. The calculated values of λ_{45} and $\lambda_{\perp}$ were also plotted. A good agreement was obtained between calculation and measurement in case of λ_{45}, justifying the calculation method adopted. A significant thermal anisotropy was identified with the highest thermal conductivity values in the direction parallel to bedding, the smallest ones in the direction perpendicular to bedding and the values in-between at 45°. This is consistent with the results reported by Dao et al. (2014a) on Boom Clay: the thermal conductivity in the horizontal direction was found to be higher than in the

231 vertical direction. Moreover, the thermal conductivity along three directions (λ_0,
232 λ_{45}, λ_{90}) increased with the increase of dry density (Figs. 2a and 2c), but decreased
233 with the increase of water content (Figs. 2b and 2d). This is commonly explained by
234 the thermal conductivities of soil components (Tang et al., 2008): the thermal
235 conductivity of solids (λ_s is equal to 7.7 W/(m.k) for quartz and 2.0 W/(m.k) for other
236 minerals) is much higher than that of water (λ_w = 0.57 W/(m.k)). Tang et al. (2008)
237 worked on compacted MX80 bentonite and they also observed that the thermal
238 conductivity increased with the increase of dry density and decreased with the
239 increase of water content.

240 Figs. 3(a)-3(b) show the changes of degree of thermal conductivity anisotropy η_T
241 with dry density and water content for samples AUB1011 and AUB1012. It appears
242 that η_T varied from 1.49 to 1.65 for samples AUB1011 and from 1.23 to 1.55 for
243 samples AUB1012. In addition, the degree of thermal conductivity anisotropy slightly
244 decreased with dry density, but slightly increased with water content.

245

246 *Compressibility and hydraulic conductivity*

247 Fig. 4 presents the compression curves of samples AUB1012 in two directions and at
248 two depths. It can be observed that slight swells occurred during saturation under the
249 in-situ vertical stress σ'_{vo} for the four samples, suggesting that the in-situ stresses were
250 slightly underestimated. By approximating each curve with two straight lines, the
251 compression indexes C_{c1} (corresponding to the common rebounding index C_s) at
252 lower stress and the compression indexes C_{c2} (corresponding to the common

253 compression index C_c) at higher stress were determined. Meanwhile, the yield stresses
254 σ'_y (corresponding to the common pre-consolidation pressure σ_p') were determined as
255 indicated by arrows in the figure. A degree of compression index anisotropy could be
256 then defined either by η_{Cc1} (ratio of C_{c1} in the vertical direction to C_{c1} in the horizontal
257 direction) or by η_{Cc2} (ratio of C_{c2} in the vertical direction to C_{c2} in the horizontal
258 direction). Similarly, the degree of yield stress anisotropy $\eta_{\sigma'_y}$ was defined as the σ'_y
259 in the horizontal direction divided by the one in the vertical direction. These
260 parameters are reported in Table 3. The C_{c1} and C_{c2} in the horizontal direction were
261 found to be slightly lower than in the vertical direction, while opposite phenomenon
262 was observed in terms of yield stress. For sample AUB1012 at 11.56 m, the η_{Cc1} and
263 $\eta_{\sigma'_y}$ were respectively 2.14 and 1.86, while for sample AUB1012 at 30.5 m and 30.8 m,
264 the two parameters were respectively equal to 2.43 and 2.21. Interestingly, the values
265 of η_{Cc2} were much lower, close to 1, indicating that after yield, the vertical sample had
266 similar compressibility with the horizontal one.

267 The hydraulic conductivity k of Teguline clay in two directions and at two depths
268 are shown in Fig. 5. For samples at 11.56 m, the logarithm of hydraulic conductivity
269 almost linearly increased with the void ratio in two directions. A significant hydraulic
270 conductivity anisotropy was evidenced, with higher values in the horizontal direction.
271 Further examination showed that for AUB 1012 at 11.56 m, the distance between the
272 lines in two directions gradually decreased after yielding, suggesting that the
273 microstructures of the vertical sample and the horizontal one were getting closer. This
274 phenomenon was not clear for AUB 1012 at 30.50 m and 30.80 m. A degree of

hydraulic conductivity anisotropy can be then defined either by η_{k1} (ratio of k_1 in the horizontal direction to k_1 in the vertical direction at the same void ratio) before the yield stress or by η_{k2} (ratio of k_2 in the horizontal direction to k_2 in the vertical direction at the same void ratio) after the yield stress. For samples AUB1012 at 11.56 m, the η_{k1} and η_{k2} were respectively 1.73 and 1.5, while for samples AUB1012 at 30.5 m and 30.8 m, owing to the limited data before the yield stress in the horizontal direction, only η_{k2} could be determined, which was about 2.0. This hydraulic conductivity anisotropy was also identified on Boom Clay (Yu et al., 2011): a η_{κ} of 1.86 was obtained with a hydraulic conductivity in the horizontal direction (6.5×10^{-12} m/s), higher than in the vertical direction (3.5×10^{-12} m/s).

In order to investigate the coupling effect between compressibility and permeability, the compression and hydraulic conductivity results are presented together in Fig. 6 in terms of normalized void ratio e/e_0 and normalized hydraulic conductivity k/k_0 versus the logarithm of vertical stress σ'_v for samples AUB1012 at 11.56 m (Fig. 6(a)) and AUB1012 at 30.5 m, 30.8 m (Fig. 6(b)). The yield stresses in two directions are also indicated on the compression curves. It can be observed from Fig. 6(a) that: i) the normalized void ratio e/e_0 decreased with the vertical stress σ'_v in two directions and the decrease of e/e_0 in the vertical direction was found to be higher than in the horizontal direction; ii) the normalized k/k_0 decreased with the vertical stress σ'_v in two directions; a linear curve was observed in the vertical direction, while a nearly bi-linear curve was identified in the horizontal direction: when the stress was lower than a threshold stress of 1.91 MPa (higher than the corresponding yield stress

297 of 1.04 MPa), the decrease of k/k_0 was small, and when the stress was higher than
298 1.91 MPa, the decrease of k/k_0 was significantly larger; iii) upon loading below the
299 threshold stress of 1.91 MPa, the decrease of k/k_0 in the horizontal direction was lower
300 than in the vertical direction, which was consistent with the corresponding variation
301 of e/e_0 versus σ'_v; by contrast, beyond the threshold stress of 1.91 MPa, the decrease
302 of k/k_0 in the horizontal direction was higher than in the vertical direction, which was
303 opposite to the corresponding variation of e/e_0 versus σ'_v, indicating that significant
304 microstructure changes occurred upon loading beyond the threshold stress of 1.91
305 MPa for the horizontal sample. The similar phenomena were observed for the samples
306 at depths 30.5 m and 30.8 m (in Fig. 6(b)).
307

308 # Discussion

309 *Thermal conductivity*

310 As mentioned previously, quartz has significantly higher thermal conductivity than
311 other minerals. Thus, the global thermal conductivity of soil λ_s is controlled by the
312 volumetric fractions of quartz and other minerals, as follows (Tang et al., 2008):

313 $$\lambda_s = \lambda_q^{v_q} \lambda_o^{1-v_q} \quad (8)$$

314 where λ_q and λ_o are respectively the thermal conductivities of quartz (7.7 W/(m.K))
315 and other minerals (2.0 W/(m.K)). v_q is the volumetric fraction of quartz.

316 The thermal conductivity of soil also depends significantly on the arrangement of
317 particles (Mcgaw, 1969; Hadley et al., 1984). Many models were used to predict the

thermal conductivity (Mcgaw, 1969; Hadley et al., 1984), among which the series model which assumes perpendicular arrangement of conduction layers and the parallel model which assumes parallel arrangement of conduction layers allowed the lower and upper bounds of thermal conductivities to be defined, as follows:

$$\lambda_{series}^{-1} = n\lambda_w^{-1} + (1-n)\lambda_s^{-1} \quad (9)$$

$$\lambda_{parallel} = n\lambda_w + (1-n)\lambda_s \quad (10)$$

where n is the soil porosity; λ_w and λ_s are respectively the thermal conductivities of water and soil solid, expressed in W/(m.K).

Fig. 7 presents the comparisons of thermal conductivities between the calculated (using the Eqs. (8), (9) and (10)) and the measured values. It is worth noting that, the measured λ_0 and calculated $\lambda_\perp$ (using Eq. (1) based on the measured λ_0 and λ_{90}) were considered as the measured values in the directions parallel and perpendicular to the bedding plane, respectively. In the calculation, the thermal conductivities of quartz, other minerals and water were taken equal to 7.7 W/(m.K), 2.0 W/(m.K) and 0.57 W/(m.K), respectively (Tang et al., 2008). The volumetric fractions of quartz, clay content were determined from Fig. 1 and the soil porosities were calculated from the dry densities (in Table 1). All results of samples AUB1011 and AUB1012 are considered in the analysis. The thermal conductivity results in Fig. 7(a) show that the series model gave satisfactory results, in particular while considering the quartz effect. On the contrary, the parallel model gave underestimation without considering the quartz effect and gave overestimation with consideration of quartz effect.

Basically, in case of series model, heat flow took place through water, quartz and other minerals in series in the direction perpendicular to the bedding plane. In that case as less solid contacts could be expected, a lower thermal conductivity was obtained. In the case of parallel model, heat flow took place through water quartz and other soil minerals in the direction parallel to the bedding plane. As more solid contacts were involved in that case, a higher thermal conductivity was expected. The satisfactory results given by the series model with consideration of quartz effect (in Fig. 7(a)) suggests that the volumetric fraction of quartz was important to be accounted for. However, it appears that the parallel model with consideration of the quartz effect overestimated the thermal conductivity (in Fig. 7(b)); thus in that case it seems more suitable to not consider the quartz effect. In fact, the real soil arrangement was neither fully in series, nor fully in parallel. Thus, in the case of series model the consideration of quartz effect compensated the effect of soil particles and water that are not in series, while in the case of parallel model the non-consideration of quartz effect compensated to some extent the effect of soil particles and water that are not in parallel.

Compressibility and hydraulic conductivity

Basically, compression in oedometer obeys K_0 condition. The value of K_0 can be estimated using the following equation (Della Vecchia et al., 2010; Lima et al., 2011; Zhang et al., 2018):

$$K_0^{SC} = (1 - sin\,\varphi')\sqrt{\mathrm{OCR}} \quad (11)$$

where K_o^{SC} is the earth pressure coefficient at rest for over-consolidation soil, φ' is the effective internal friction angle, OCR is the over-consolidation ratio. For Teguline clay extracted at 11.56 m and 30.5 m, the OCRs are respectively 4.5 and 5.3 (determined from Fig. 4), and the effective internal friction angle φ' is about 27.3° (Zhang et al., 2018). The K_o^{SC} values determined using Eq. (11) are respectively 1.15 and 1.24 for samples extracted at 11.56 m and 30.5 m, indicating that the maximum effective stress that Teguline clay had suffered in the horizontal direction in the history was expected to be higher than in the vertical direction. This is the reason why the yield stress in the horizontal direction was higher than in the vertical direction.

The degrees of anisotropy identified in terms of thermal conductivity, compression index, yield stress and hydraulic conductivity are not far from each other for the studied Teguline clay: η_T varied from 1.23 to 1.65, η_{Cc1} from 2.14 to 2.43, $\eta_{\sigma'y}$ from 1.86 to 2.21 and η_{k1} was 1.73. This indicates that bedding is a good indicator of thermo-hydro-mechanical anisotropy for natural stiff clays.

The compression curves (see Fig. 4) and hydraulic conductivities (see Fig. 5) in the horizontal and the vertical directions were found to gradually converge after yield, suggesting that the hydro-mechanical anisotropy of the horizontal sample was approaching that of the vertical one. As the microstructure of soil does not change significantly before the yield stress, the anisotropy identified represents the inherent one. On the contrary, significant microstructure change can be expected beyond the yield stress and in that case any anisotropy identified represents the induced one. Thereby, the large values of η_{Cc1}, $\eta_{\sigma'y}$ and η_{k1} obtained suggest a significant inherent

383 anisotropy of Teguline clay, in agreement with the results of thermal conductivity.
384 Upon loading beyond the yield stress, similar values of compression index C_{c2} in two
385 directions (see Table 3) were obtained. This does not indicate an isotropic behaviour;
386 it just suggests that the microstructures of the vertical sample and the horizontal one
387 were getting closer after yielding. The evolution of microstructure for vertical and
388 horizontal Teguline clay samples during loading can be described in Fig. 8. For the
389 vertical sample, loading in oedometer after the yield stress led to more and more
390 anisotropic microstructure feature because of the expected increase of particle
391 orientation (Delage and Lefebvra, 1984; Cui et al., 2013), while for the horizontal
392 sample, the inherent anisotropy disappeared first upon loading; then, induced
393 anisotropy developed with the increase of particle orientation. Thus, the changes of
394 principle stresses (as if rotation of principal stresses took place) was involved in that
395 case and the horizontal sample experienced changes from initial inherent anisotropy
396 to isotropy and then to the stress-induced anisotropy.

397 The microstructure changes during loading for vertical and horizontal samples
398 described in Fig. 8 were in agreement with the evolution of k/k_0 with σ'_{vo} in
399 semi-logarithmic plot (Figs. 6(a) and 6(b)). For the horizontal sample, the decrease of
400 k/k_0 with σ'_{v} was small before the threshold stress, as the fluid flow in the direction
401 parallel to the bedding is dominant and in that case the bedding plane acts as
402 preferential path for water flow. By contrast, beyond the threshold stress, dramatic
403 decrease of k/k_0 was observed, indicating that inherent anisotropy disappeared and
404 induced anisotropy appeared with the increase of particle orientation. In that case,

405 water flow in the direction normal to the induced orientated particles became
406 prevailing. Thereby, for the horizontal sample, the threshold stress identified in the
407 k/k_0 - σ'_v curve in semi-logarithmic plot separated the zone with prevailing parallel
408 flow (in the direction parallel to the inherent bedding plane) from the zone with
409 prevailing perpendicular flow (in the direction perpendicular to the induced orientated
410 particles). This threshold stress should correspond to the stress that generated the
411 isotropic state in the soil. For the vertical sample, no clear threshold stress was
412 observed in the k/k_0-σ'_v curve in semi-logarithmic plot. This is logical because loading
413 in oedometer after the yield stress led to more and more anisotropy and in that case
414 the changes of perpendicular flow (in the direction perpendicular to the bedding plane
415 before the yield stress and normal to the induced orientated particles after the yield
416 stress) were dominant.
417

418 ## Conclusion

419 The anisotropy feature of stiff Teguline clay was investigated in terms of thermal
420 conductivity, compressibility and hydraulic conductivity. The results obtained allow
421 the following conclusions to be drawn.

422 A significant thermal conductivity anisotropy was evidenced: the highest value
423 was in the direction parallel to the bedding plane and the smallest one in the direction
424 perpendicular to the bedding plane, the one at 45° being logically in between, in
425 agreement with the results of hydraulic conductivity. The compression index also
426 revealed the anisotropic feature of Teguline clay: lower values were identified in the

427 horizontal direction. Moreover, the clay anisotropy was also characterized by higher
428 values of yield stress in the horizontal direction than in the vertical direction.

429 The degrees of thermal conductivity anisotropy η_T, compression index
430 anisotropy η_{Cc1}, the yield stress anisotropy $\eta_{\sigma'_y}$ and hydraulic conductivity anisotropy
431 η_{k1} were not far from each other, suggesting that bedding is a good indicator of the
432 inherent thermo-hydro-mechanical anisotropy for natural stiff clays.

433 Upon loading in oedometer, the inherent anisotropic features of Teguline clay
434 changed after the yield stress: for the vertical sample, loading led to more and more
435 particle orientation and thus more and more anisotropy. On the contrary, for the
436 horizontal sample, loading led to the disappearance of the inherent anisotropy first,
437 before creating the stress-induced anisotropy. The evolution of k/k_0 versus σ'_{vo} in
438 semi-logarithmic plot also was found to be in agreement with the microstructure
439 changes.

440 These findings confirm that natural stiff clays, through their formation by
441 deposition, develop orientated microstructure. As a result, anisotropic features
442 develop in terms of thermal conductivity, compressibility and hydraulic conductivity.
443 These anisotropic features changed upon loading beyond the yield stress or the
444 threshold stress. This anisotropy feature is important to be accounted for when
445 constructing geotechnical and geo-environmental structures in natural stiff clays.

446

447 # References

448 AFNOR., 1997. Sols: reconnaissance et essais. Essais oedométriques. Partie 1: Essai
449 de compressibilité sur matériaux fins quasi saturés avec chargement par paliers.

Alshawmar, F., 2014. Evaluation of compressibility, anisotropy and at-rest lateral earth pressure in Champlain Sea clays. Master thesis, University of Ottawa. Ottawa, Canada.

Armand, G., Noiret, A., Zghondi, J., Seyedi, D.M., 2013. Short- and long-term behaviors of drifts in the Callovo-Oxfordian claystone at the Meuse/Haute-Marne Underground Research Laboratory. J Rock Mech Geotech Eng. 5, 221-230.

ASTM D5334-00, 2000. Standard test methods for determining of thermal conductivity of soil and soft rock by thermal needle probe procedure. ASTM International, West Conshohocken, PA.

Bertrand, F., Collin, F., 2017. Anisotropic modelling of Opalinus Clay behaviour: From triaxial tests to gallery excavation application. J Rock Mech Geotech Eng. 9(3), 435-448.

Cui, Y.J., Nguyen, X.P., Tang, A.M., Li, X.L., 2013. An insight into the unloading/reloading loops on the compression curve of natural stiff clays. Appl. Clay Sci. 83-84, 343-348.

Davis, M.G., Chapman, D.S., Van Wagoner, T.M., Armstrong, P.A., 2007. Thermal conductivity anisotropy of metasedimentary and igneous rocks. J. Geophys. Res. 112 (B05216), 1-7.

Dao, L.Q., Delage, P., Tang, A.M., Cui, Y.J., Pereira, J.M., 2014a. Anisotropic thermal conductivity of natural Boom Clay. Appl. Clay Sci. 101, 282-287.

Dao, L.Q., Cui, Y.J., Tang, A.M., Pereira, J.M., Li, X.L., Sillen, X., 2014b. Investigating the anisotropy of the shear modulus of natural Boom Clay. Geotech Lett. 4, 98-101.

Dao, L.Q., Cui, Y.J., Tang, A.M., Delage, P., Li, X.L., Sillen, X., 2015a. Anisotropy in Oedometer Test on Natural Boom Clay. Engineering Geology for Society and Territory. 6, 499-502.

Dao, L.Q., Cui, Y.J., Tang, A.M., Pereira, J.M., Li, X.L., Sillen, X., 2015b. Impact of excavation damage on the thermo-hydro-mechanical properties of natural Boom Clay. Eng Geol. 195, 196-205.

Delage, P., Lefebvre, G., 1984. Study of the structure of a sensitive Champlain clay and of its evolution during consolidation. Can. Geotech J. 21(1), 21-35.

Delage, P., Le, T.T., Tang, A.M., Cui, Y.J., Li, X.L., 2007. Suction and in-situ stresses of deep Boom clay samples. Géotechnique. 57(1), 239-244.

Della Vecchia, G., Lima, A., Jommi, C., and Romero, E. 2010. Some remarks on the hydro-mechanical constitutive modelling of natural and compacted Boom clay. Proc. 5th Int. Conf. on Unsaturated Soils. Barcelona. Taylor and Francis Group, London, 803-809.

Farouki, O.T., 1986. Thermal properties of soils. Rock and Soil Mechanics 11. Trans Tech Publications, Clausthal-Zellerfeld, Germany.

Favero, V., Ferrari, A., Laloui, L., 2018. Anisotropic behaviour of Opalinus Clay through consolidated and drained triaxial testing in saturated conditions. Rock Mech Rock Eng. 51(5), 1305-1319.

Francois, B., Labiouse, V., Dizier, A., Marinelli, F., Charlier, R., Collin, F., 2014.

494 Hollow Cylinder Tests on Boom Clay: Modelling of Strain Localization in the
495 Anisotropic Excavation Damaged Zone. Rock Mech Rock Eng. 47, 71-86.
496 Hadley, G.R., Mcvey, D.F., Morinl, R., 1984. Thermophysical properties of deep
497 ocean sediments. Marine Geotechnology. 5(3-4), 257-295.
498 Hicher, Y.P., Wayudi, H., Tessier, D., 2000. Microstructural analysis of inherent and
499 induced anisotropy in clay. Mech Cohes-frict Mat. 5(5), 341-371.
500 Johansen, O., 1975. Thermal conductivity of soils. Ph.D. thesis, Trondheim, Norway.
501 (CRREL Draft Translation 637, 1977). ADA 044002.
502 Khan, M.M.A., 1993. Strength-deformation behaviour of a weathered clay crust. PhD
503 thesis, University of Ottawa, Ottawa, Canada.
504 Lima, A., Romero, E., and Piña, Y. 2011. Water retention properties of two deep
505 Tertiary clay formations within the context of radioactive waste disposal. VII
506 Brazilian Symposium on Unsaturated Soil. Pirenópolis, Goiania, Brazil,
507 315-321.
508 Masri, M., Sibai, M., Shao, J.F., Mainguy, M. 2014. Experimental investigation of the
509 effect of temperature on the mechanical behavior of Tournemire shale. Int J Rock
510 Mech Min Sci. 70, 185-191.
511 Mcgaw, R., 1969. Heat conduction in saturated granular materials. High research
512 board sepcial report. 103, 114-131.
513 Midttømme, K., Roaldset, E., 1999. Thermal conductivity of sedimentary rocks:
514 uncertainties in measurement and modeling. Geol. Soc. Lond., Spec. Publ.
515 158(1), 45-60.
516 Munroe, R.J., Sass, J.H., 1987. Thermal Conductivity of Samples From Borehole
517 VC-1, Report 87-184. Geological Survey.
518 Naumann, M., Hunsche, U., Schulze, O., 2007. Experimental investigations on
519 anisotropy in dilatancy, failure and creep of Opalinus Clay. Phys. Chem. Earth.
520 32(8-14), 889-895.
521 Niandou, H., Shao, J.F., Henry, J.P., Fourmaintraux, D., 1997. Laboratory
522 investigation of the mechanical behaviour of Tournemire shale. Int J Rock Mech
523 Min Sci. 34(1), 3-16.
524 Penner, E., 1963. Anisotropic thermal conduction in clay sediments. International
525 Clay Conference.
526 Popov, Y., Bayuk, I., Parshin, A., Miklashevskiy, D., Novikov, S., Chekhonin, E.,
527 2012. New methods and instruments for determination of reservoir thermal
528 properties. Proceedings Thirty-seventh Workshop on Geothermal Reservoir
529 Engineering. Stanford University, Stanford, California.
530 Riche, F., Schneebeli, M., 2013. Thermal conductivity of snow measured by three
531 independent methods and anisotropy considerations. The Cryosphere. 7,
532 217-227.
533 Salehnia, F., Collin, F., Li, X.L., Dizier, A., Sillen, X., Charlier, R., 2015. Coupled
534 modeling of Excavation Damaged Zone in Boom clay: Strain localization in rock
535 and distribution of contact pressure on the gallery's lining. Comput Geotech. 69,
536 396-410.
537 Seyedi, D.M., Armand, G., Noiret, A., 2017. "Transverse Action"- A model

benchmark exercise for numerical analysis of the Callovo-Oxfordian claystone hydromechanical response to excavation operations. Comput Geotech. 85, 287-305.
Tang, A.M., Cui, Y.J., Le, T.T., 2008. A study on the thermal conductivity of compacted bentonites. Appl. Clay Sci. 41, 181-189.
Ye, W.M., Lu, Y., Huang, X.H., Chen, B., Chen, Y.G., Cui, Y.J., 2017. Anisotropic thermal conductivity of unsaturated compacted GMZ bentonite-sand mixture. PanAm Unsaturated Soils. 413-424.
Yu, L., Gedeon, M., Wemaere, I., Marivoet, J., De Craen, M., 2011. Boom clay hydraulic conductivity. A Synthesis of 30 Years of Research. External Report SCK-CEN, Mol (Belgium).
Zhang, C.L., Armand, G., Conil, N., 2015. Investigation on the anisotropic mechanical behaviour of the Callovo-Oxfordian clay rock. Final report.
Zhang, F., Cui, Y.J., Zeng, L.L., Robinet, J.C., Conil, N., Talandier, Jean., 2018. Effect of degree of saturation on the uncondined compressive strength of natural stiff clays with consideration of air entry value. Eng. Geol. 237, 140-148.
Zeng, L.L., Cui, Y.J., Conil, N., Zghondi, J., Armand, G., Talandier, J., 2017. Experimental study on swelling behaviour and microstructure changes of natural stiff clays upon wetting. Can. Geotech J. 54(5), 700-709.

List of Tables

Table 1. Program for thermal conductivity tests
Table 2. Program for compressibility and hydraulic conductivity tests
Table 3. Parameters obtained from the compression curves

List of Figures

Fig. 1. Variations of (a) clay content; (b) quartz content over depth
Fig. 2. Variations of thermal conductivity with (a) dry density for samples AUB1011; (b) water content for samples AUB1011; (c) dry density for samples AUB1012; (d) water content for samples AUB1012
Fig. 3. Variations of degree of thermal conductivity anisotropy η_T with (a) dry density; (b) water content
Fig. 4. Compression curves
Fig. 5. Hydraulic conductivity k versus void ratio e
Fig. 6. Normalized e/e_0 or k/k_0 versus vertical stress σ'_{v0} for samples (a) AUB1012 at 11.56 m; (b) AUB1012 at 30.5 m and 30.8 m
Fig. 7. Comparisons of measured thermal conductivity and calculated values by (a)

series model; (b) parallel model

Fig. 8. Conceptual model for vertical sample and horizontal sample subjected to loading in one-dimensional condition

Table 1. Program for thermal conductivity tests

Core	Depth(m)	Water content (%)	Dry density (Mg/m^3)	Direction
AUB1011	18.21	13.68	1.98	0°, 45° and 90°
	31.76	12.13	2.04	0°, 45° and 90°
AUB1012	5.46	19.53	1.74	0°, 45° and 90°
	11.56	15.28	1.87	0°, 45° and 90°
	18.06	14.69	1.90	0°, 45° and 90°
	30.5	12.20	2.04	0°, 45° and 90°
	31.22	12.19	2.06	0°, 45° and 90°

606 **Table 2**. Program for compressibility and hydraulic conductivity tests

Core	Depth(m)	Direction	Stress path (MPa)
AUB1012	11.56	Horizontal Vertical	0.125-0.375-0.874-1.874-3.872-7.869
	30.8	Horizontal	0.345-0.594-1.094-2.093-4.092-8.089-16.083
	30.5	Vertical	

607 Note that the horizontal direction refers to the loading direction parallel to the bedding
608 plane, while the vertical direction refers to the loading direction normal to the bedding
609 plane.

610

611 **Table 3.** Parameters obtained from the compression curves

Core	Direction	C_{C1}	η_{Cc1}	σ'_y	$\eta_{\sigma' y}$	C_{C2}	η_{Cc2}
AUB1012 11.56 m	Horizontal	0.0081	2.14	1.04	1.86	0.074	1.09
	Vertical	0.0173		0.56		0.081	
AUB1012 30.8 m	Horizontal	0.0042	2.43	3.97	2.21	0.064	1.14
AUB1012 30.5 m	Vertical	0.0102		1.80		0.073	

612
613
614
615
616
617

618

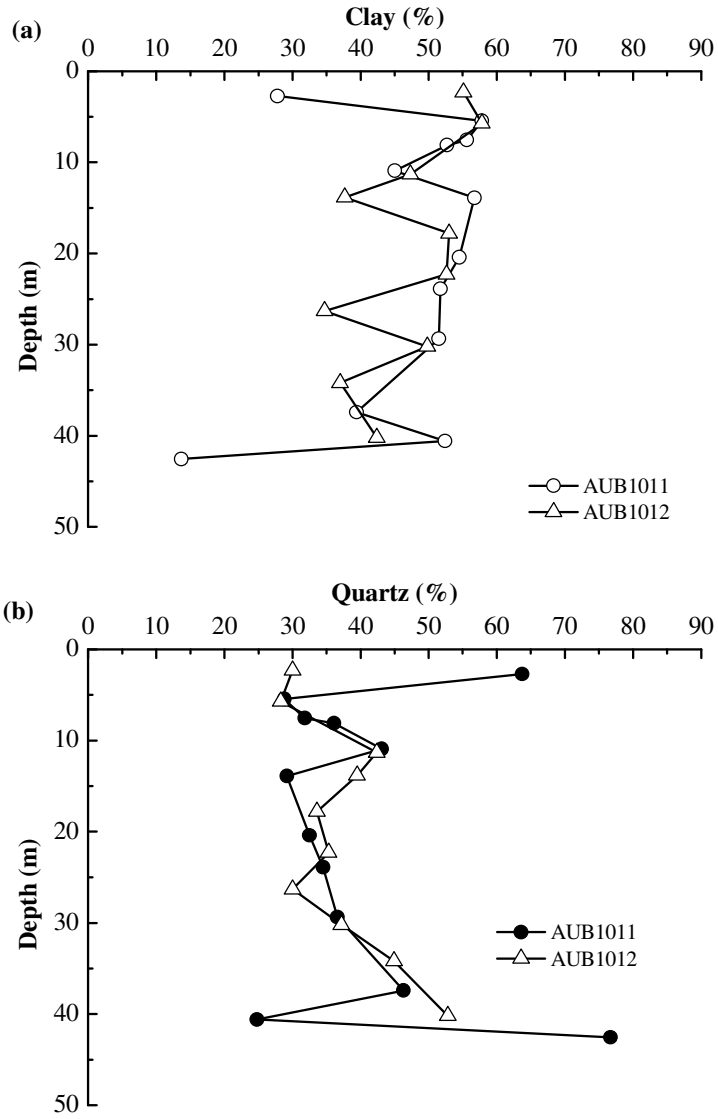

619

620 **Fig. 1.** Variations of (a) clay content; (b) quartz content over depth

621

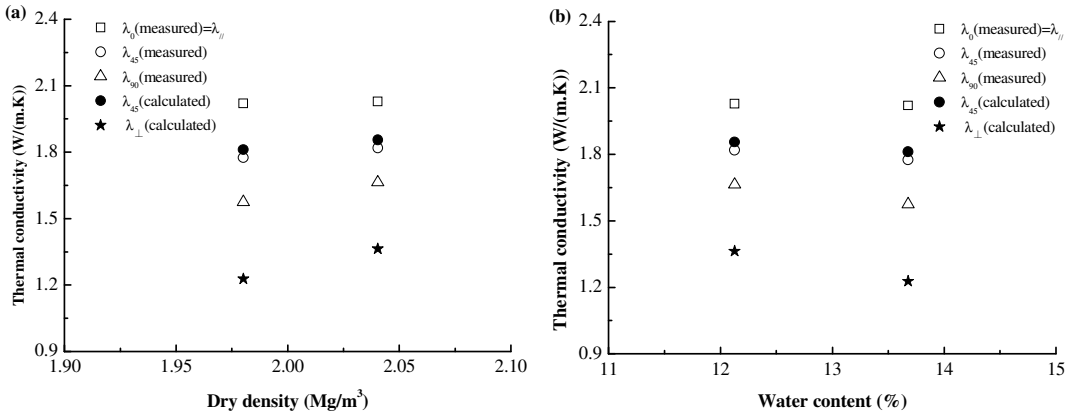

622

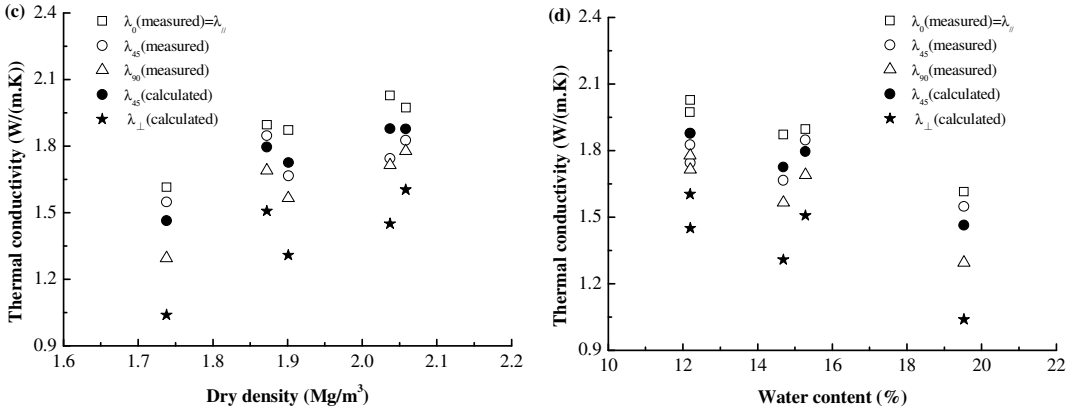

Fig. 2. Variations of thermal conductivity with (a) dry density for samples AUB1011; (b) water content for samples AUB1011; (c) dry density for samples AUB1012; (d) water content for samples AUB1012

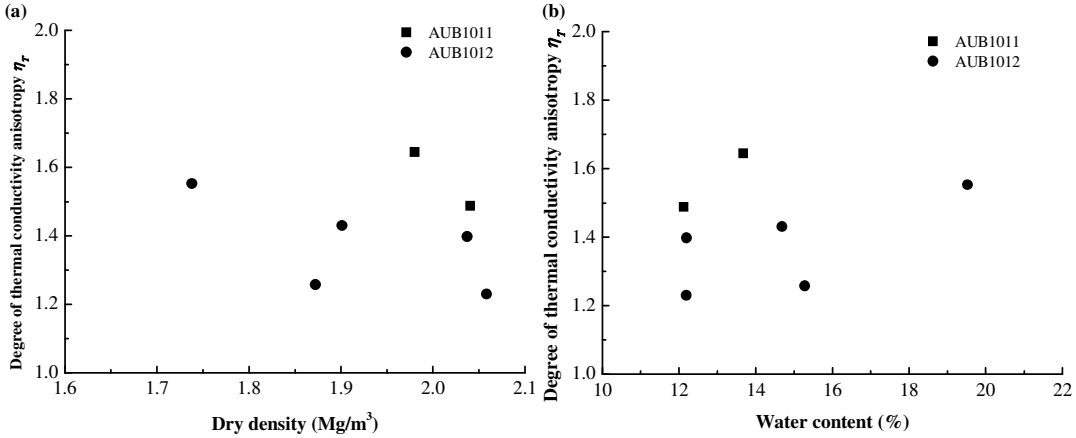

Fig. 3. Variations of degree of thermal conductivity anisotropy η_T with (a) dry density; (b) water content

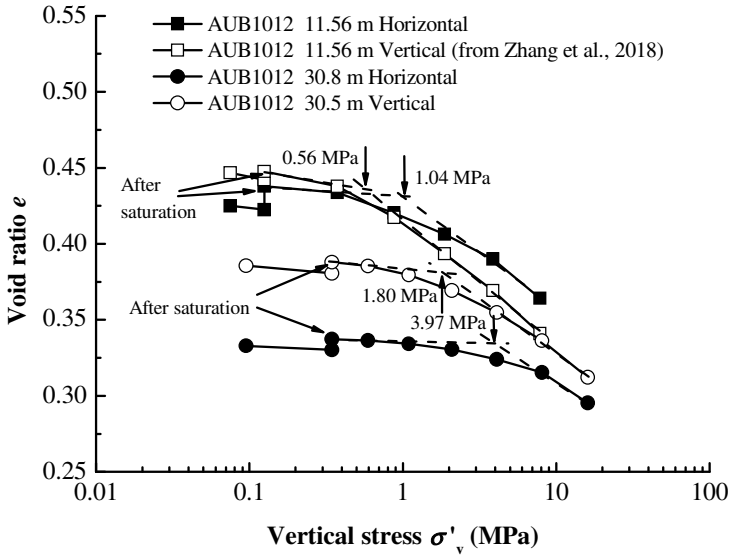

Fig. 4. Compression curves

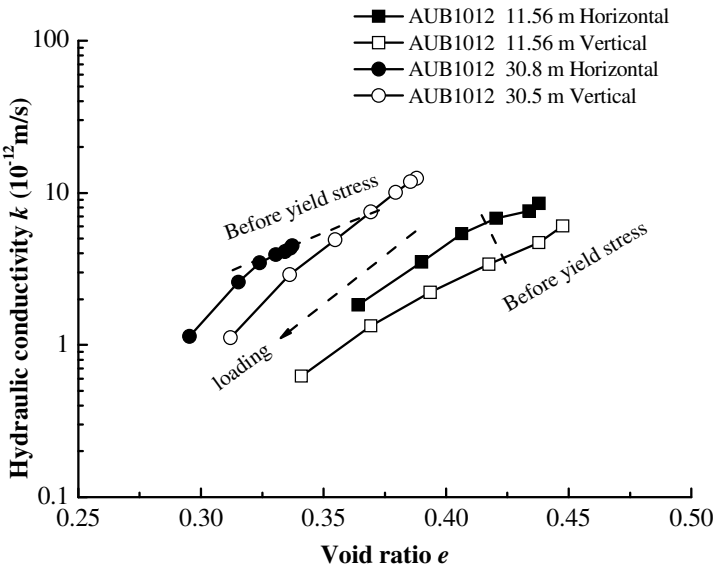

632

633 **Fig. 5.** Hydraulic conductivity *k* versus void ratio *e*

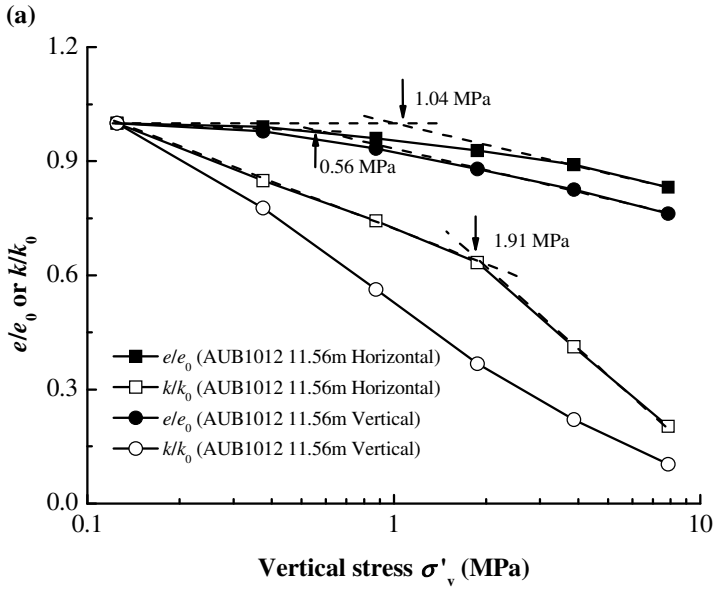

634

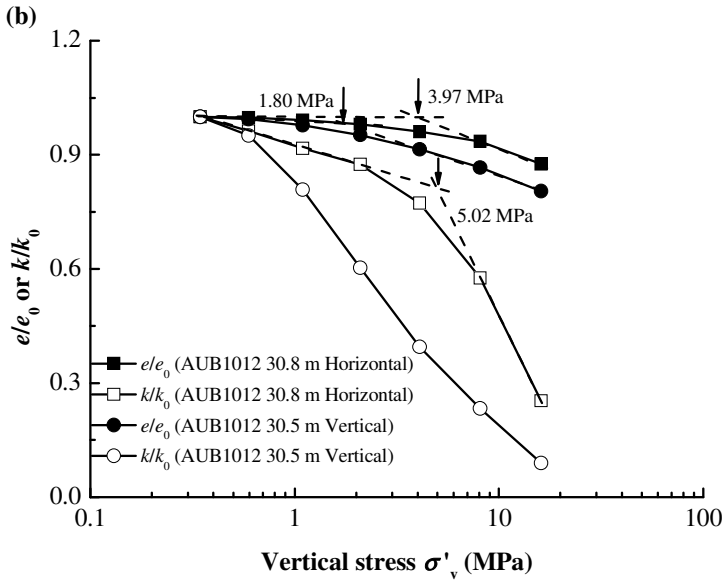

635

636 **Fig. 6.** Normalized e/e_0 or k/k_0 versus vertical stress σ'_{v0} for samples (a) AUB1012 at
637 11.56 m; (b) AUB1012 at 30.5 m and 30.8 m

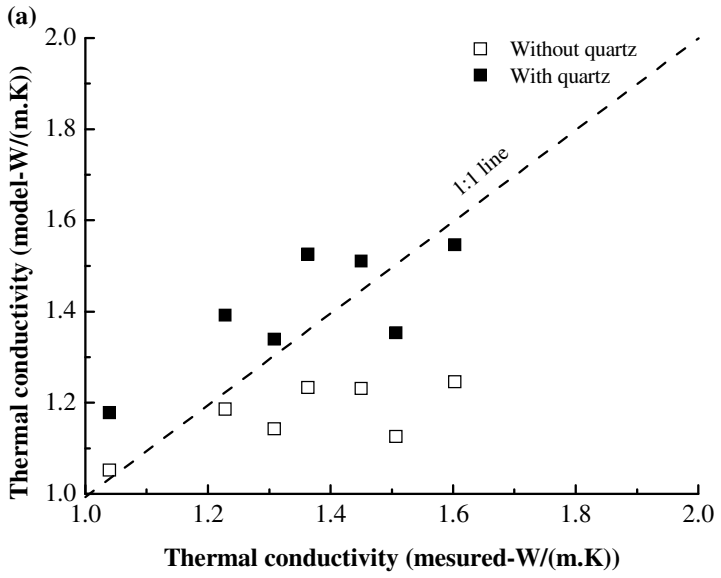

638

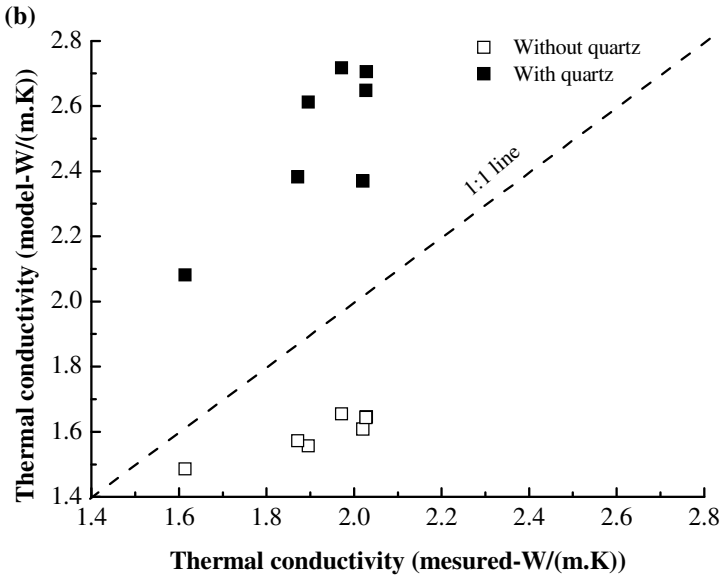

639

640 **Fig. 7.** Comparisons of measured thermal conductivity and calculated values by (a)
641 series model; (b) parallel model

642

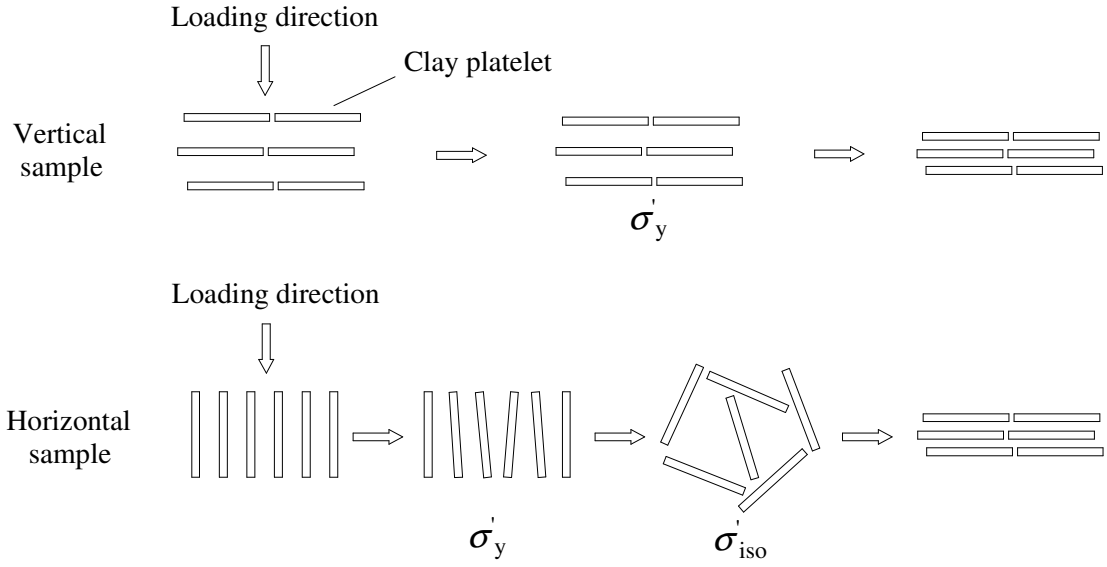

643

644 **Fig. 8.** Conceptual model for vertical sample and horizontal sample subjected to
645 loading in one-dimensional condition

646